Elastic constants of solid ^{4}He under pressure: Diffusion Monte Carlo study

C. Cazorla,[1] Y. Lutsyshyn,[2] and J. Boronat[3]

[1]*Institut de Ciència de Materials de Barcelona (ICMAB-CSIC), ES-08193 Bellaterra, Spain*

[2]*Institut für Physik, Universität Rostock, DE-18051 Rostock, Germany*

[3]*Departament de Física i Enginyeria Nuclear, Universitat Politècnica de Catalunya, Campus Nord B4-B5, ES-08034, Barcelona, Spain*

(Received 20 July 2011; revised manuscript received 21 December 2011; published 4 January 2012)

We study the elasticity of perfect solid ^{4}He at zero temperature using the diffusion Monte Carlo method and a realistic semiempirical pairwise potential to describe the He-He interactions. We calculate the value of the elastic constants of hcp helium $\{C_{ij}\}$ as a function of pressure from zero up to ∼110 bar. It is found that the pressure dependence of all nonzero elastic constants is linearly increasing and we provide accurate parametrization of each of them. Our C_{ij} results are compared to previous variational calculations and low-temperature measurements and, in general, we find notably good agreement among them. Furthermore, we report results for the Grüneisen parameters, sound velocities, and Debye temperature over a wide range of pressures. This work represents a comprehensive quantum atomistic calculation of the elastic properties of solid helium under compression.

DOI: 10.1103/PhysRevB.85.024101 PACS number(s): 67.80.−s, 02.70.Ss

I. INTRODUCTION

The behavior of solid ^{4}He and of quantum crystals in general (e.g., H_2 and Ne) is exceptionally so rich that, despite having been investigated for more than about eight decades, it is to this day not yet completely understood. One example of helium's intriguing nature is its elasticity. Experimental studies on the elastic properties of hcp ^{4}He were already conducted by Wanner, Crepeau, and Greywall in the early 1970s.[1–3] Those original works consisted of a series of sound-velocity measurements performed at thermodynamic conditions relatively close to the stability domain of the liquid, namely, $T \sim 1$ K and $25 \leqslant P \leqslant 50$ bar. With the advance of cryogenic technology and crystal growth techniques, it is now possible to analyze practically defect-free ^{4}He samples at just a few mK in the laboratory. Recently, Beamish and collaborators have developed an experimental technique that has allowed them to measure directly the shear modulus μ of hcp ^{4}He under extremely low strains and frequencies.[4,5] The temperature dependence of μ within the temperature interval $0.01 \leqslant T \leqslant 0.5$ K has been determined, and a striking resemblance with nonclassical rotational inertia (NCRI) data obtained in torsional oscillator experiments[6,7] has been unraveled. Specifically, the value of the NCRI and shear modulus increases, respectively, about 1–10% and 2% as the temperature is lowered down to 0.01 K. While the findings of Beamish *et al.* have been initially explained in terms of pinning (unpinning) of dislocations induced by the presence of static (mobile) ^{3}He impurities,[4,8–10] it remains to be clarified whether the cited experimental similarities must be regarded simply as coincidental or are in fact related to the onset of supersolidity.[11–13]

Simulation techniques have been demonstrated as invaluable tools for predicting and accurately characterizing the energetic and structural properties of quantum solids.[14–22] Nevertheless, computational studies on the elasticity of solid ^{4}He are sparse to date. To the best of our knowledge, there exist only two recent works in which the shear modulus of solid helium has been explicitly calculated from first principles.[23,24] This computational scarcity strongly contrasts with research done in other fields such as classical solid-state theory or high-pressure physics, where estimation of the elastic properties of materials (e.g., strain-stress tensor, Grüneisen parameters, vibrational phonon frequencies, etc.) is a standard.[25–28] The likely explanation for such a contrast (aside from no particular interest in the matter prior to the findings of Beamish *et al.*[4,5]) are the difficulties encountered in modeling of bosonic quantum effects, namely, atomic exchanges and anharmonicity. These quantum atomic effects are indeed crucial to comprehend the physical nature of solid ^{4}He at low temperatures and, as a matter of fact, they can not be reproduced correctly within customary quasiharmonic approaches.[29–31]

In this work, we present a computational study of the elastic properties of perfect (e.g., free of defects) solid ^{4}He in the hcp structure based on the diffusion Monte Carlo approach. This study is intended to improve our understanding of the response of solid helium to external strain at zero temperature, and further extends the work initiated by Pessoa *et al.*[23] In particular, we provide the dependence of helium elastic constants and related quantities (e.g., sound velocities, Grüneisen parameters, and Debye temperature) on pressure up to ∼110 bar. This is a significantly higher pressure than previously considered both experimentally and theoretically. Our results are compared to experimental data and other calculations when available and, as it will be shown later on, good agreement is generally found among them. The computational method that we employ is fully quantum and virtually exact, that is, in principle only affected by statistical uncertainties. In this sense, our work also represents an improvement with respect to previous first-principles work[23] based on variational Monte Carlo calculations (i.e., subject to bias stemming from the choice of the trial wave function).

The remainder of this paper is structured as follows. In Sec. II, we review the basics of elasticity in hcp crystals and provide the details of our computational methodology. In the following section, we present our results along with some discussions. Finally, we summarize the main conclusions and comment on prospective work in Sec. IV.

II. THEORY AND COMPUTATIONAL DETAILS

A. Elastic constants

For small strains, the zero-temperature energy of a crystal can be expressed as

$$E = E_0 + \frac{1}{2} V_0 \sum_{i,j=1}^{6} C_{ij} s_i s_j, \tag{1}$$

where V_0 and E_0 are the volume and internal energy of the undistorted solid, $\{C_{ij}\}$ the elastic constants, and $\{s_i\}$ the strain components defined such that s_1, s_2, and s_3 are fractional increases in the x, y, and z directed axes, and s_4, s_5, and s_6 angular increases of the xy, xz, and yz angles.[32–34] The symmetry properties of the crystal under consideration define the number of elastic constants that are nonzero. In hcp crystals, this number reduces to five, namely, C_{11}, C_{12}, C_{33}, C_{13}, and C_{44}, where C_{44} is commonly known as the shear modulus.[35] In order to calculate these nonzero elastic constants, it is necessary to compute the second derivative of the internal energy of the crystal with respect to the strain tensor σ_{ij}. For this, the hcp crystal must be considered in hexagonal symmetry, that is, expressed in terms of its unit cell with primitive translational vectors $\mathbf{a_1} = a(+\frac{1}{2}\mathbf{i} + \frac{\sqrt{3}}{2}\mathbf{j})$, $\mathbf{a_2} = a(-\frac{1}{2}\mathbf{i} + \frac{\sqrt{3}}{2}\mathbf{j})$, and $\mathbf{a_3} = c\mathbf{k}$ (where a and c are the lattice parameters in the basal plane and along the z axis, respectively, and $\mathbf{i}$, $\mathbf{j}$, and $\mathbf{k}$ correspond to the usual unitary Cartesian vectors), and two-atom basis set $\mathbf{r_1} = \frac{1}{3}\mathbf{a_1} - \frac{2}{3}\mathbf{a_2} + \frac{1}{4}\mathbf{a_3}$ and $\mathbf{r_2} = \frac{2}{3}\mathbf{a_1} - \frac{1}{3}\mathbf{a_2} + \frac{3}{4}\mathbf{a_3}$ (see Fig. 1).

The relationships between strain and the elastic constants $\{C_{ij}\}$ in a hcp crystal were determined in the past within the framework of elasticity theory. These are[32–34]

$$K = -V\left(\frac{\partial P}{\partial V}\right)_{V=V_0} = \frac{C_{33}(C_{11}+C_{12}) - 2C_{13}^2}{C_0} \tag{2}$$

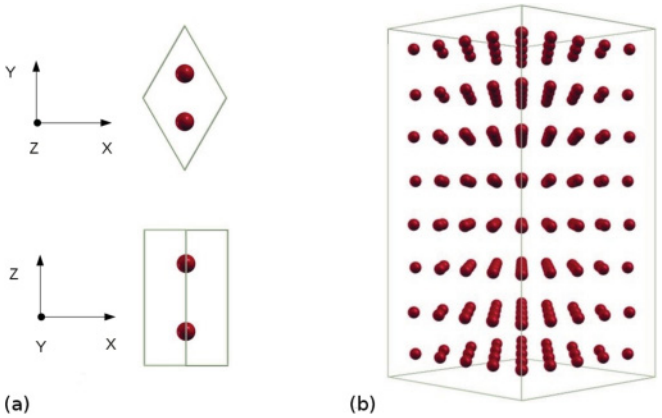

FIG. 1. (Color online) (a) Representation of the hcp unit cell with primitive translational vectors $\mathbf{a_1}$, $\mathbf{a_2}$, and $\mathbf{a_3}$, and two-atom basis set (see text). (b) Sketch of the 200-atom supercell used in the pure shear calculations, which is built in by replicating the hcp unit cell $5 \times 5 \times 4$ times along the primitive translational vectors $\mathbf{a_1}$, $\mathbf{a_2}$, and $\mathbf{a_3}$, respectively.

and

$$-V\left(\frac{\partial \ln c/a}{\partial V}\right)_{V=V_0} = \frac{C_{33} - C_{11} - C_{12} + C_{13}}{C_0}, \tag{3}$$

with

$$C_0 = C_{11} + C_{12} + 2C_{33} - 4C_{13}. \tag{4}$$

In addition, one defines

$$C_{66} = \tfrac{1}{2}(C_{11} - C_{12}) \tag{5}$$

and C_{44}.

Equations (2) and (3) correspond to homogeneous strains that change the volume and shape of the hcp unit cell. The dependence of pressure P and c/a ratio on volume can be readily obtained from standard equation-of-state calculations. On the other hand, quantities C_0, C_{66}, and C_{44} represent the response of the crystal to heterogeneous strains that keep the volume of the hcp unit cell fixed. In order to calculate the value of these pure shears, it is necessary to compute the variation of the internal energy of the equilibrium structures with respect to certain crystal deformations. These crystal deformations can be expressed as transformed primitive translational vectors,[34] which in the C_0 case are

$$\begin{aligned}
\mathbf{a_1}^0 &= a\phi^{-1}\left(+\frac{1}{2}\mathbf{i} + \frac{\sqrt{3}}{2}\mathbf{j}\right),\\
\mathbf{a_2}^0 &= a\phi^{-1}\left(-\frac{1}{2}\mathbf{i} + \frac{\sqrt{3}}{2}\mathbf{j}\right),\\
\mathbf{a_3}^0 &= c\phi^2\mathbf{k},
\end{aligned} \tag{6}$$

where $\phi = (1+\eta)^{1/2}$ is a dimensionless parameter and $C_0 = \frac{2}{V_0}(\frac{\partial^2 E}{\partial \eta^2})_{V=V_0}$ (the equilibrium condition is satisfied at $\eta = 0$). For C_{66}, we have

$$\begin{aligned}
\mathbf{a_1}^{66} &= a\gamma^{1/2}\left(+\frac{1}{2}\mathbf{i} + \gamma^{-1}\frac{\sqrt{3}}{2}\mathbf{j}\right),\\
\mathbf{a_2}^{66} &= a\gamma^{1/2}\left(-\frac{1}{2}\mathbf{i} + \gamma^{-1}\frac{\sqrt{3}}{2}\mathbf{j}\right),\\
\mathbf{a_3}^{66} &= c\mathbf{k},
\end{aligned} \tag{7}$$

where γ is also a dimensionless parameter and $C_{66} = \frac{1}{V_0}(\frac{\partial^2 E}{\partial \gamma^2})_{V=V_0}$ (the equilibrium condition is now satisfied at $\gamma = 1$). And finally, for C_{44},

$$\begin{aligned}
\mathbf{a_1}^{44} &= a\left(+\frac{1}{2}\mathbf{i} + \frac{\sqrt{3}}{2}\mathbf{j} + \frac{\epsilon}{2}\mathbf{k}\right),\\
\mathbf{a_2}^{44} &= a\left(-\frac{1}{2}\mathbf{i} + \frac{\sqrt{3}}{2}\mathbf{j} - \frac{\epsilon}{2}\mathbf{k}\right),\\
\mathbf{a_3}^{44} &= c\mathbf{k},
\end{aligned} \tag{8}$$

where again a dimensionless parameter ϵ is introduced and $C_{44} = \frac{1}{V_0}(\frac{\partial^2 E}{\partial \epsilon^2})_{V=V_0}$ (the equilibrium condition corresponds to $\epsilon = 0$).

Once the value of the bulk modulus K and quantities $\partial \ln(c/a)/\partial V$, C_0, C_{66}, and C_{44} are determined, one can

calculate the corresponding $C_{ij} \neq 0$ hcp elastic constants straightforwardly by solving the nonlinear system of equations defined by Eqs. (2)–(5).

B. Diffusion Monte Carlo

The grounds of the diffusion Monte Carlo (DMC) method have been reviewed with detail in other works,[36–39] so we recall here only the essential ideas. In the DMC approach, the time-dependent Schrödinger equation of a quantum system of N interacting particles is solved stochastically by simulating the time evolution of the Green's function propagator $e^{-\frac{i}{\hbar}\hat{H}t}$ in imaginary time $\tau \equiv \frac{it}{\hbar}$. For $\tau \to \infty$, sets of configurations (walkers) $\{\mathbf{R}_i \equiv \mathbf{r}_1, \ldots, \mathbf{r}_N\}$ rendering the probability distribution function $(\Psi_0\Psi)$ are generated, where Ψ_0 is the true ground-state wave function of the system and Ψ the trial wave function used for importance sampling. Within DMC, virtually exact results (i.e., subject to statistical uncertainties only) are obtained for the total ground-state energy and related quantities of bosonic quantum systems.[40–42] It is worth noticing that despite the fact that asymptotic DMC values do not depend on the choice of the trial wave function, the algorithmic efficiency is greatly affected by the quality of Ψ.

We are interested in studying the ground state of perfect hcp ^{4}He, which we assume to be governed by the Hamiltonian $H = -\frac{\hbar^2}{2m_{\mathrm{He}}}\sum_{i=1}^{N}\nabla_i^2 + \sum_{i<j}^{N} V_{\text{He-He}}(r_{ij})$, where m_{He} is the mass of a ^{4}He atom, N the number of particles, and $V_{\text{He-He}}$ the semiempirical pairwise potential due to Aziz *et al.*[43] It is worth noting that this two-body potential provides an excellent description of the He-He interactions, including weak long-ranged van der Waals forces, over all the pressure ranges considered in this work.[17,44]

The trial wave function that we use for importance sampling Ψ_{SNJ} simultaneously reproduces crystal ordering and Bose-Einstein symmetry[45] (that is, remains unchanged under the permutation of atoms). This model wave function was recently introduced in Ref. 46 and it reads

$$\Psi_{\mathrm{SNJ}}(\mathbf{r}_1, \ldots, \mathbf{r}_N) = \prod_{i<j}^{N} f(r_{ij}) \prod_{J=1}^{N} \left(\sum_{i=1}^{N} g(r_{iJ}) \right), \qquad (9)$$

where the index in the second product runs over perfect lattice position vectors (sites). In previous works, we have shown that Ψ_{SNJ} provides an excellent description of the ground-state properties of bulk hcp ^{4}He (Ref. 46) and quantum solid films.[18,22,47] The key ingredient for this progress is the Ψ_{SNJ} localization factor [second term in Eq. (9)], which is constructed in such a way that voids originated by multiple occupancy of a same site are energetically penalized. Correlation functions in Eq. (9) were adopted in the McMillan $f(r) = \exp[-1/2(b/r)^5]$ and Gaussian $g(r) = \exp[-1/2(ar^2)]$ forms. The value of the parameters in functions f and g were optimized variationally at density $\rho = 0.480\sigma^{-3}$ ($\sigma = 2.556$ Å, $b = 1.08\sigma$, and $a = 10.10\sigma^{-2}$) and used in the rest of simulations.

The technical parameters in our calculations were set in order to ensure convergence of the total energy per particle to less than 0.02 K/atom. For instance, the value of the mean population of walkers was 400 and the length of the imaginary time step $(\Delta\tau)$ 5×10^{-4} K^{-1}. Statistics were accumulated over 10^5 DMC steps performed after system equilibration, and the approximation used for the short-time Green's function $e^{-\hat{H}\tau}$ is exact up to order $(\Delta\tau)^2$.[39,48]

C. Computational strategy

In order to work out Eq. (2), we used the bulk modulus volume dependence reported in Ref. 49, where the equation of state of hcp ^{4}He was already calculated employing the DMC method and considering accurate finite-size corrections to the total energy.[17] Prior to this, we performed a series of geometry optimizations at each volume aimed at determining the value of the corresponding equilibrium c/a ratio (that is, the one that minimizes the ground-state energy). We found that regardless of the pressure considered, the optimal c/a value was always 1.63(1) (so that the equation of state reported in Ref. 49 could be used for our present purposes without any concern; we also note that our optimal c/a ratio result is consistent with previous first-principles calculations performed by other authors[50]). Consequently, the left-hand side of Eq. (3) vanishes and the solution to the system of equations defined by (2)–(5) reduces to

$$\begin{aligned} C_{11} &= K + C_{66} + \tfrac{1}{18}C_0, \\ C_{12} &= K - C_{66} + \tfrac{1}{18}C_0, \\ C_{13} &= K - \tfrac{1}{9}C_0, \\ C_{33} &= K + \tfrac{2}{9}C_0. \end{aligned} \qquad (10)$$

The simulation box used in our pure shear calculations contains 200 ^{4}He atoms and was generated by replicating the hcp unit cell five times along the $\mathbf{a_1}$ and $\mathbf{a_2}$ directions, and four times along the c axis (see Fig. 1). In proceeding so, hexagonal symmetry in our supercell calculations is guaranteed by construction. Periodic boundary conditions were imposed across the three directions defined by the edges of the nonorthorhombic simulation box.

The value of the second derivatives involved in the computation of the elastic constants were obtained following the next strategy. For each volume and pure shear considered, first we calculated the total energy per particle in a series of supercells generated by incrementally distorting the equilibrium geometry according to the translational lattice vectors (6)–(8). Up to eight different and equally spaced shear increments were considered for each volume, taking both positive and negative values within the intervals $-0.15 \leqslant \epsilon \leqslant 0.15$, $-0.10 \leqslant \gamma - 1.0 \leqslant 0.10$, and $-0.20 \leqslant \eta \leqslant 0.20$. Subsequently, the series of shear-dependent total energies so obtained were fitted to a third-order polynomial function of the form $f(x) = a + bx^2 + cx^3$ (we note that second-order polynomial curves provided identical elastic constants results to which we are going to present next). In all the cases, we found that the optimal a, b, and c values reproduced the series of calculated total energies per particle within their statistical errors (see Fig. 2). In the calculations involving pure shear strains, the volume of the cell was kept constant by construction [see Eqs. (6)–(8)]. Therefore, performing the correction due

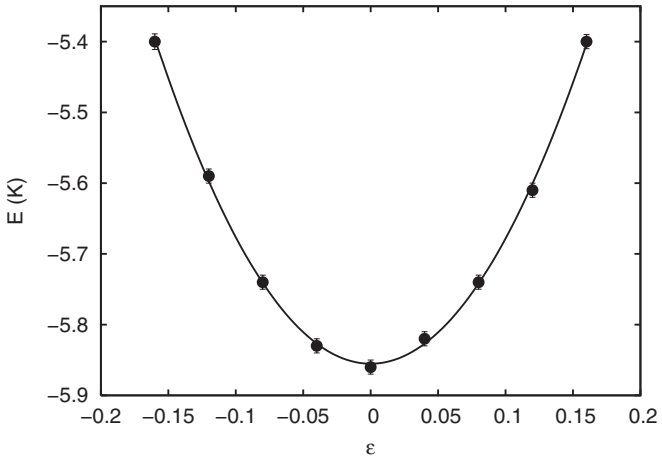

FIG. 2. Energy per particle results obtained by varying the degree of shear stress, as defined in Eq. (8), in perfect hcp ^{4}He at density $\rho = 0.480\sigma^{-3}$. The equilibrium value corresponding to the undistorted hcp structure is found at $\epsilon = 0$ and the solid line represents a third-order polynomial fit to the energies. Statistical uncertainties in the energies are represented with error bars.

to finite size of the system was not necessary, as it would not affect the second derivatives used for the computation of the elastic constants. We shall stress that this is not the case in bulk modulus and $\partial \ln(c/a)/\partial V$ calculations where the volume of the simulation cell is varied and, consequently, accurate energy corrections for the finite-size effects are required.

III. RESULTS AND DISCUSSIONS

A. Elastic constants

In Figs. 3, 4, and 5, we show the pressure dependence of the five elastic constants of perfect hcp ^{4}He as obtained in our calculations. The error bars δC_{ij} in our results, stemming from both statistical uncertainties in the energies and corresponding third-order polynomial fits, typically amount to $\delta C_{ij}/C_{ij} \sim 2\%$. We found that the pressure variation of all nonzero elastic constants is monotonically increasing and practically linear within all the studied range. Consequently, we performed fits of the $C_{ij}(P) = a_{ij} + b_{ij}P$ form to our results (see Figs. 3, 4, and 5) and report the value of the resulting a_{ij} and b_{ij} coefficients in Table I. It is observed that the most sensitive elastic constant to pressure changes is C_{33}, whereas C_{44} is the least (see b_{ij} values in Table I). We checked that our results fulfill the requirements of mechanical stability in hcp crystals under arbitrary pressure, namely, $0 \leqslant C_{ij}$, $0 \leqslant C_{11} - C_{12}$, $0 \leqslant C_{11} + C_{33} - 2C_{13}$, and $0 \leqslant 2C_{11} + C_{33} + 2C_{12} - 4C_{13}$.[33] Also, we note that the mechanical stability of the hcp phase is further enhanced with compression as shown by the monotonic increasing behavior of all calculated C_{ij}'s.

Comparison between our DMC calculations, previous variational Monte Carlo (VMC) results, and experimental data is also provided in Figs. 3–5. VMC results reported at $P \sim 34$ bar[23] have been obtained by Pessoa *et al.* using a shadow wave-function model (SWF).[51] This type of trial wave function correctly accounts for the atomic Bose-Einstein statistics, is translationally invariant, and so far it has yielded the most

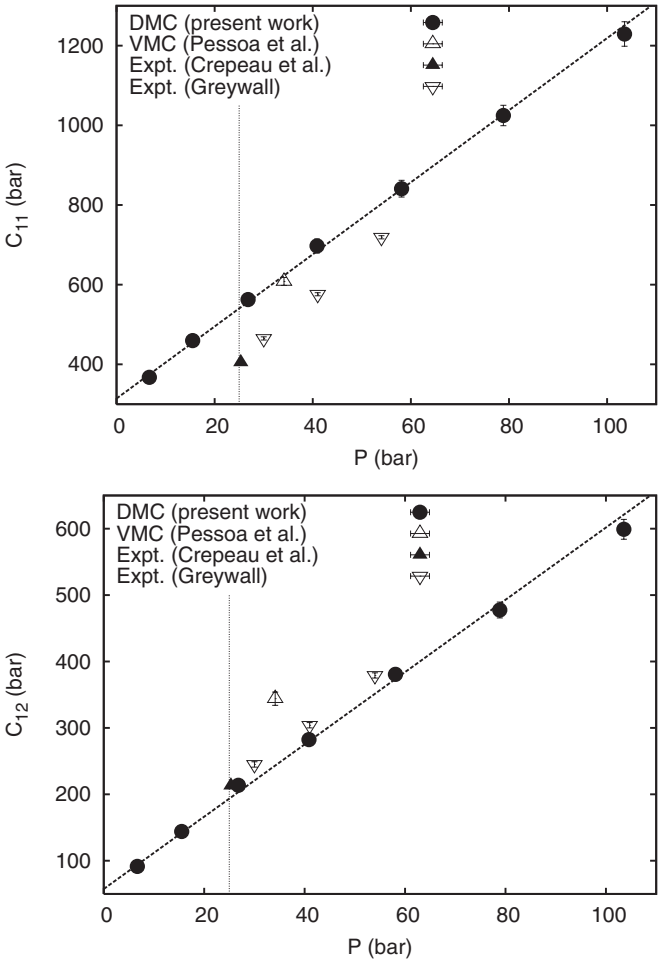

FIG. 3. Zero-temperature C_{11} and C_{12} elastic constants of perfect hcp ^{4}He as a function of pressure. Previous variational Monte Carlo (VMC) calculations (Ref. 23) and experimental data (Refs. 2 and 3) are shown for comparison. The vertical dotted line represents the zero-temperature freezing pressure of ^{4}He and the straight dashed lines are linear fits to the DMC results (see text).

accurate variational description of solid helium.[52] Arguably, Pessoa's VMC predictions are in fairly good agreement with our DMC results since in general relation $|C_{ij}^{\rm VMC} - C_{ij}^{\rm DMC}|/C_{ij}^{\rm DMC} \leqslant 10\%$ is fulfilled with the only exception of C_{12} (in that case, however, measurements appear to follow closely to our results). Recalling that evaluation of C_{ij}'s requires the computation of the total energy second derivatives, it can be said that the satisfactory DMC-VMC agreement found further corroborates the excellent variational quality of the SWF model.

Regarding the experimental data taken from Refs. 2 and 3, we also find good agreement (see Figs. 3–5). The sound-velocity measurements performed by Crepeau and Greywall involved high-quality single helium crystals, the basal plane orientations of which were accurately determined using x rays. Consequently, our modest discrepancies with Crepeau and Greywall's data are very likely to be originated by remanent crystal defects and thermal excitations (we recall that the temperature in those experiments was $\sim$1 K). We note that our C_{44} results also reproduce closely recent ^{4}He shear

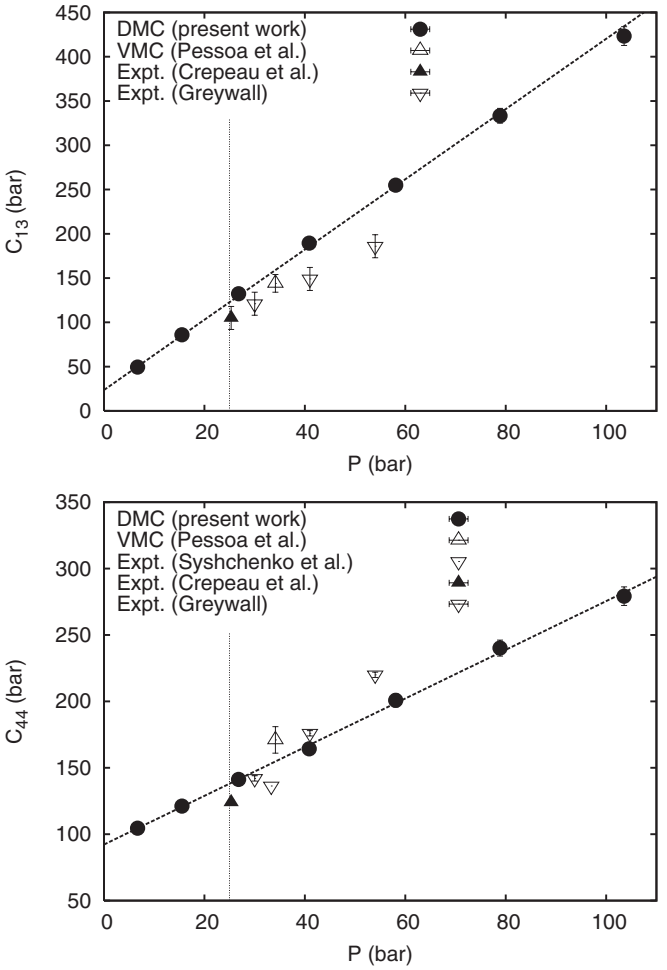

FIG. 4. Zero-temperature C_{13} and C_{44} elastic constants of perfect hcp ^{4}He as a function of pressure. Previous variational Monte Carlo (VMC) calculations (Ref. 23) and experimental data (Refs. 2, 3, and 5) are shown for comparison. The vertical dotted line represents the zero-temperature freezing pressure of ^{4}He and the straight dashed lines are linear fits to the DMC results (see text).

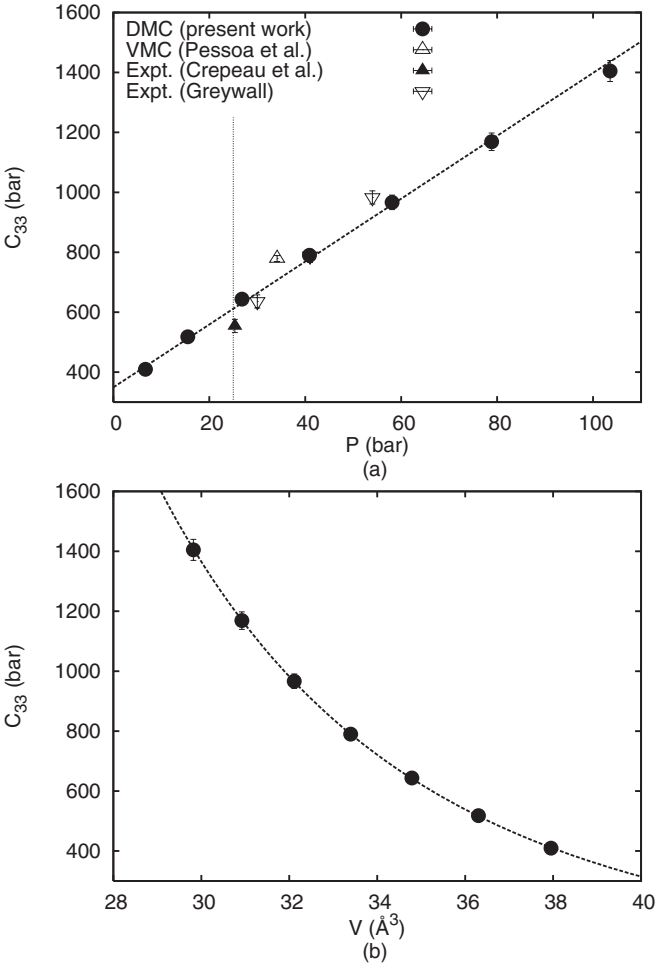

FIG. 5. (a) Zero-temperature C_{33} elastic constant of perfect hcp ^{4}He as a function of pressure. A previous variational Monte Carlo (VMC) calculation (Ref. 23) and experimental data (Refs. 2 and 3) are shown for comparison. The vertical dotted line represents the zero-temperature freezing pressure of ^{4}He and the straight dashed line is a linear fit to the DMC results (see text). (b) Dependence of the C_{33} elastic constant on volume. The dashed line represents a power-law fit to the DMC results from which the value of the corresponding Grüneisen parameter is obtained (see text).

modulus measurements performed by Beamish *et al.*[4,5] (see Fig. 4). In Sec. III B, we will comment again on the possible origins of the small discrepancies found with experiments, however, it can be already claimed that the manifested overall good agreement between our C_{ij} calculations and $30 \leqslant P \leqslant 60$ bar experiments appears to endorse the reliability of our computational approach.

Another quantity of interest in the study of crystal elasticity is the Grüneisen parameter $\hat{\gamma}$. This parameter quantifies how atomic vibrations in a crystal are affected by changes in volume and customarily is defined as $\hat{\gamma} = (V/C_v)\beta K$, where C_v stands for the specific heat and β for the thermal expansion coefficient. However, this definition is not practical for low-temperature calculations since in general quantities C_v and β tend to zero similarly near $T = 0$, thus leading to large numerical errors. Alternatively, Klein *et al.*[53] derived a Grüneisen parameter expression that is valid in the zero-temperature limit and that depends on the individual vibrational frequency modes. Specifically, Klein's expression can be reformulated in terms of the elastic constants as[3]

$$\gamma_{ij} = -\frac{1}{2}\frac{\partial \ln C_{ij}}{\partial \ln V} - \frac{1}{6}. \tag{11}$$

According to this formula, the volume dependence of each C_{ij} elastic constant can be fitted to a function of the form

$$C_{ij}(V) = A\left(\frac{V}{V_0}\right)^{-(\frac{1}{3}+2\gamma_{ij})}, \tag{12}$$

TABLE I. Value of the parameters obtained in the linear fits to our $C_{ij}(P)$ results (see text). Typical a_{ij} (expressed in units of bar) and b_{ij} (dimensionless) uncertainties amount to 1%.

	C_{11}	C_{12}	C_{13}	C_{33}	C_{44}
a_{ij}	314.26	57.45	23.59	349.22	92.19
b_{ij}	9.05	5.44	3.97	10.49	1.83

from which one can readily extract the value of the corresponding γ_{ij} parameter. We proceeded in this way using the C_{ij} results obtained in our $0 \leqslant P \leqslant 110$ bar simulations (see Fig. 5) and got $\gamma_{11} = 2.34(5)$, $\gamma_{12} = 3.69(5)$, $\gamma_{13} = 4.23(5)$, $\gamma_{33} = 2.70(5)$, and $\gamma_{44} = 1.91(5)$, where the numerical uncertainties are expressed within parentheses. The averaged Grüneisen parameter $\hat{\gamma} = \frac{1}{5}\sum \gamma_{ij}$ corresponding to our results is 2.67(5), where the summation runs over indexes 11, 12, 33, 44, and 66 ($\gamma_{66} = 2.70$ as obtained from C_{66}) since the respective elastic constants are the quantities that are directly measured in sound-velocity experiments.[3] Our $\hat{\gamma}$ value compares very well with Greywall's experimental result of 2.7. We must note, however, that in our calculations the differences $|\gamma_{ij} - \hat{\gamma}|$ are in general nonzero. It is worth comparing the value of the zero-temperature Grüneisen parameter of solid ^{4}He to that of other rare-gas species. We know from Ref. 54 that $\hat{\gamma}$ is 2.5 in Ne, 2.7 in Ar, 2.7 in Kr, and 2.5 in Xe. Consequently, the elastic constants of all five noble gases will vary very similarly upon a same change of volume. The same conclusion, however, does not apply to pressure since the corresponding bulk moduli are appreciably different.

In order to quantify the importance of quantum effects in our study, we computed the contribution of the potential and kinetic energies to the shear modulus (C_{44}^p and C_{44}^k, respectively). For this, we carried out simulations at density $\rho = 0.480\sigma^{-2}$ in which the *exact* value of the second derivative of the potential energy E^p with respect to strain was calculated using the pure estimator technique.[42] The kinetic energy contribution to the shear modulus C_{44}^k was subsequently obtained by subtracting the quantity $C_{44}^p = \frac{1}{V_0}(\frac{\partial^2 E^p}{\partial \epsilon^2})_{V=V_0}$ to C_{44}. (We checked that the strain dependence of E^k could also be accurately fitted to a third-order polynomial function.) In fact, the zero-temperature C_{44}^k value of a classical crystal exactly amounts to zero since the atoms there remain totally frozen in the perfect lattice positions (that is, $C_{44}^p = C_{44}$). Even in the case of considering quasiharmonic zero-point motion corrections to C_{44}, C_{44}^k is not expected to depart significantly from zero. In contrast, we found that in perfect hcp ^{4}He, C_{44}^p/C_{44} amounts to 68%, or conversely, $C_{44}^k/C_{44} = 32\%$. This last result evidences the quantum nature of helium's elasticity and demonstrates the inability of classical and quasiharmonic approaches to reproduce it.

B. Sound velocities

Sound velocities in solids, either longitudinal or transverse, depend on the direction of propagation. In crystals with hexagonal symmetry, two main propagation modes are identified, one along the c axis (defined by vector $\mathbf{a_3}$ in Sec. II A) and the other contained within the basal plane (defined by vectors $\mathbf{a_1}$ and $\mathbf{a_2}$ in Sec. II A). The relationships between the elastic constants and sound velocities in hcp crystals are[55,56]

$$\begin{aligned} v_L &= (C_{33}/\rho)^{1/2}, \\ v_{T1} &= (C_{44}/\rho)^{1/2}, \\ v_{T2} &= (C_{44}/\rho)^{1/2} \end{aligned} \qquad (13)$$

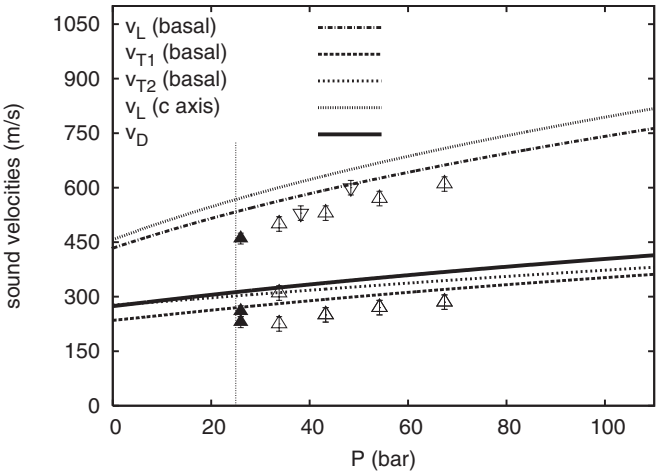

FIG. 6. Pressure dependence of the longitudinal (L) and transvere (T) sound velocities of hcp ^{4}He along its corresponding c axis and basal plane. v_D represents the averaged Debye velocity (see text). Basal sound-velocity data from Refs. 3 (△), 2 (▲), and 1 (▽) are shown for comparison. The vertical dotted line represents the zero-temperature freezing pressure of ^{4}He.

along the c axis, and

$$\begin{aligned} v_L &= (C_{11}/\rho)^{1/2}, \\ v_{T1} &= (C_{66}/\rho)^{1/2}, \\ v_{T2} &= (C_{44}/\rho)^{1/2} \end{aligned} \qquad (14)$$

within the basal plane.

In Fig. 6, we plot the pressure dependence of the transverse and longitudinal sound velocities of hcp ^{4}He as obtained from our C_{ij} results reported in Sec. III A. The error bars in our results, not shown in the figure, are $\delta v_{L,T}/v_{L,T} \sim 1\%$. It is observed that at compressions far beyond freezing, all sound velocities increase almost linearly with pressure. In contrast, the longitudinal c axis and basal components appear to follow a certain power law within the low-pressure interval $0 \leqslant P \leqslant 25$ bars (metastable regime). Certainly, the nature of the sound propagation modes in metastable solid ^{4}He, either at positive or negative pressures, is poorly understood at present in spite of its fundamental physical interest.[57] It is our aim to report in detail on this topic in the future, so we leave discussions on this matter out of this work.

Experimental longitudinal and transverse basal sound velocities are shown for comparison in Fig. 6. The agreement between those measurements and our results is generally good (in fact, within the same relative margin as reported in the previous section for the elastic constants). Specifically, our predicted sound velocities are systematically a bit larger than those values reported by Wanner,[1] Crepeau,[2] and Greywall.[3] Such a systematic overestimation is consistent with our previous suggestion that certain thermal effects, not included in our simulations, could be affecting the experiments. As a matter of fact, the more a material is softened by effect of temperature, the slower the sound waves propagate across it. Aside from thermal effects, residual defects in the crystal samples such as dislocations could be also contributing to the observed discrepancies. Seemingly, systematic experimental

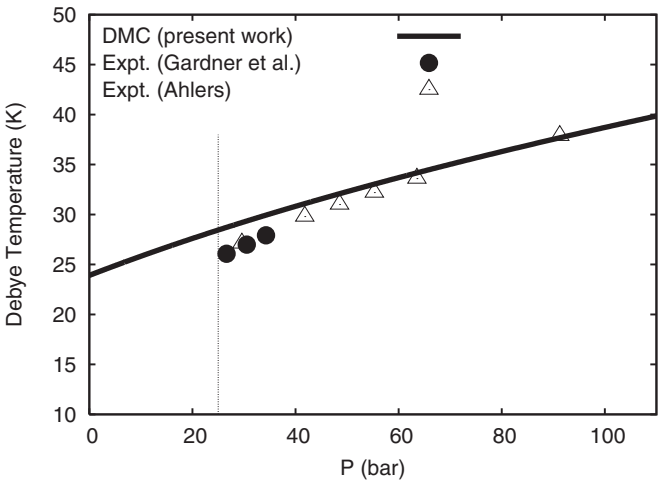

FIG. 7. $T = 0$ Debye temperature of hcp ^{4}He as a function of pressure (solid line). Experimental results from Refs. 58 and 59 are shown for comparison. The vertical dotted line represents the zero-temperature freezing pressure of ^{4}He, and the thickness of the line corresponds to the uncertainty associated to our calculations ($\delta\Theta_D/\Theta_D \sim 1\%$).

uncertainties should not be discarded either. For instance, Balibar and collaborators[10] have recently detected a possible source of error in experiments involving dilution refrigerators, which could be biasing estimation of the sound velocities in high-quality single crystals by as much as 20%. New and refined low-T sound-velocity measurements in high-quality ^{4}He monocrystals are very much desirable for improving our present understanding of this system.

In order to provide an additional, and probably more meaningful, comparison between our zero-temperature results and experiments, we calculated the $T = 0$ Debye temperature of ^{4}He Θ_D. The zero-temperature Θ_D of a crystal can be easily extrapolated from lattice heat-capacity measurements performed at low temperatures. Fortunately, results for this quantity have already been reported for helium in a wide range of pressures.[58,59] The definition of the $T = 0$ Debye temperature is

$$\Theta_D = \frac{2\pi\hbar}{k_B}\left(\frac{3}{4\pi V}\right)^{\frac{1}{3}} v_D, \tag{15}$$

where V is the volume per atom and v_D the Debye velocity. This velocity is given by

$$\frac{1}{v_D^3} = \frac{1}{3}\left(\frac{1}{\overline{v}_L^3} + 2\frac{1}{\overline{v}_T^3}\right), \tag{16}$$

where the average velocities $\overline{v}_L$ and $\overline{v}_T$ are defined by

$$\frac{1}{\overline{v}_{L,T}^3} = \left\langle \frac{1}{v_{L,T}^3} \right\rangle, \tag{17}$$

and the $\langle \cdots \rangle$ brackets denote angular averages of the longitudinal and transverse velocities. In our case, we have approximated the angular averages in Eq. (17) by

$$\frac{1}{\overline{v}_L^3} \approx \frac{1}{2}\left(\frac{1}{v_{L,b}^3}\right) + \frac{1}{2}\left(\frac{1}{v_{L,c}^3}\right) \tag{18}$$

and

$$\frac{1}{\overline{v}_T^3} \approx \frac{1}{3}\left(\frac{1}{v_{T1,b}^3}\right) + \frac{1}{3}\left(\frac{1}{v_{T2,b}^3}\right) + \frac{1}{3}\left(\frac{1}{v_{T,c}^3}\right), \tag{19}$$

where index b stands for the basal plane and index c for the c-axis direction.[60]

In Fig. 7, we plot our results for the zero-temperature Θ_D of hcp ^{4}He and experimental data taken from Refs. 58 and 59. In fact, very good agreement between the measurements of Gardner and Ahlers and our calculations is observed. This last result seems to confirm our previous suggestion that thermal effects might be affecting the agreement between our elastic constants' and sound velocities' results and experiments. Finally, we note that the pressure variation of Θ_D is very similar to that observed in the longitudinal sound-velocity components of helium, namely, almost linear at high compressions and of power-law type at lower densities.

IV. SUMMARY AND PERSPECTIVES

We have developed a fully quantum computational strategy to accurately calculate the zero-temperature elastic properties of perfect hcp ^{4}He under pressure, in particular, a complete set of the elastic constants, sound velocities, Grüneisen parameters, and the Debye temperature. Our diffusion Monte Carlo results agree with low-T sound-velocity measurements and variational first-principles calculations by other authors, and spans over a much wider pressure range than previously considered. It is found that all nonzero elastic constants of helium vary linearly with pressure within the interval $0 \leqslant P \leqslant 110$ bar, and we have provided accurate parametrization of each of them. The Grüneisen parameters, sound velocities, and $T = 0$ Debye temperature of solid helium have been also determined and compared to available experimental data. The computational method introduced in this work is completely general and can be used to study the elasticity of hcp quantum solids other than helium-4 (e.g., H_2).

It is our aim to analyze in future work the elastic behavior of ^{4}He at negative pressures using the computational technique described here. In doing this, we expect to be able to determine its spinodal density limit (that is, the density at which the elastic constants vanish) rigorously, and also characterize the pressure dependence of the transverse and basal sound velocities close to it. Also, we are interested in applying our formalism to study the ground state of defective hcp ^{4}He (for instance, by introducing vacancies), where the supersolid state of matter clearly manifests. In doing this, we expect to gather quantitative knowledge on the relationship (if any) between elasticity and supersolidity from a purely microscopic approach and so to help to understand the origins of recent shear modulus observations. Work in these directions is already in progress.

ACKNOWLEDGMENT

The authors acknowledge partial financial support from the DGI (Spain) Grant No. FIS2008-04403 and Generalitat de Catalunya Grant No. 2009SGR-1003.

[1] R. Wanner and J. P. Franck, Phys. Rev. Lett. **24**, 365 (1970).
[2] R. H. Crepeau, O. Heybey, D. M. Lee, and S. A. Strauss, Phys. Rev. A **3**, 1162 (1971).
[3] D. S. Greywall, Phys. Rev. A **3**, 2106 (1971); Phys. Rev. B **16**, 5127 (1977).
[4] J. Day and J. Beamish, Nature (London) **450**, 853 (2007).
[5] O. Syshchenko, J. Day, and J. Beamish, J. Phys.: Condens. Matter **21**, 164204 (2009).
[6] E. Kim and M. H. W. Chan, Nature (London) **427**, 225 (2004).
[7] E. Kim and M. H. W. Chan, Science **305**, 1941 (2004).
[8] J. Day, O. Syshchenko, and J. Beamish, Phys. Rev. Lett. **104**, 075302 (2010).
[9] J. Day, O. Syshchenko, and J. Beamish, Phys. Rev. B **79**, 214524 (2009).
[10] X. Rojas, A. Haziot, V. Bapst, S. Balibar, and H. J. Maris, Phys. Rev. Lett. **105**, 145302 (2010).
[11] H. Choi, D. Takahashi, K. Kono, and E. Kim, Science **330**, 1512 (2010).
[12] D. Y. Kim, H. Choi, W. Choi, S. Kwon, E. Kim, and H. C. Kim, Phys. Rev. B **83**, 052503 (2011).
[13] I. Iwasa, Phys. Rev. B **81**, 104527 (2010).
[14] P. A. Whitlock, D. M. Ceperley, G. V. Chester, and M. H. Kalos, Phys. Rev. B **19**, 5598 (1979).
[15] P. A. Whitlock, M. H. Kalos, G. V. Chester, and D. M. Ceperley, Phys. Rev. B **21**, 999 (1980).
[16] D. M. Ceperley and G. Jacucci, Phys. Rev. Lett. **58**, 1648 (1987).
[17] C. Cazorla and J. Boronat, J. Phys.: Condens. Matter **20**, 015223 (2008).
[18] C. Cazorla and J. Boronat, Phys. Rev. B **77**, 024310 (2008).
[19] J. Boronat, C. Cazorla, D. Colognesi, and M. Zoppi, Phys. Rev. B **69**, 174302 (2004).
[20] C. Cazorla and J. Boronat, J. Low Temp. Phys. **134**, 43 (2004).
[21] C. Cazorla and J. Boronat, Phys. Rev. B **78**, 134509 (2008).
[22] C. Cazorla, G. Astrakharchick, J. Casulleras, and J. Boronat, J. Phys.: Condens. Matter **22**, 165402 (2010).
[23] R. Pessoa, S. A. Vitiello, and M. de Koning, Phys. Rev. Lett. **104**, 085301 (2010).
[24] Luis Aldemar Pena Ardila, Silvio A. Vitiello, and Maurice de Koning, Phys. Rev. B **84**, 094119 (2011).
[25] C. Cazorla, D. Errandonea, and E. Sola, Phys. Rev. B **80**, 064105 (2009).
[26] G. Steinle-Neumann, L. Stixrude, and R. E. Cohen, Phys. Rev. B **60**, 791 (1999).
[27] C. Cazorla, D. Alfè, and M. J. Gillan, Phys. Rev. Lett. **101**, 049601 (2008).
[28] M. J. Gillan, D. Alfè, J. P. Brodholt, L. Vocadlo, and G. D. Price, Rep. Prog. Phys. **69**, 2365 (2006).
[29] S. Baroni, S. de Gironcoli, A. del Corso, and P. Giannozzi, Rev. Mod. Phys. **73**, 515 (2001).
[30] D. Alfè, Comput. Phys. Comm. **180**, 2622 (2009).
[31] G. Kresse, J. Furthmüller, and J. Hafner, Europhys. Lett. **32**, 729 (1995).
[32] T. H. K. Barron and M. L. Klein, Proc. Phys. Soc. **85**, 523 (1965).
[33] D. C. Wallace, *Thermodynamics of Crystals* (Wiley, New York, 1972).
[34] W. F. King and P. H. Cutler, J. Phys. Chem. Solids **32**, 761 (1971).
[35] In particular, $C_{11} = C_{22} \neq 0$, $C_{13} = C_{31} \neq 0$, $C_{12} = C_{21} \neq 0$, $C_{44} = C_{55} \neq 0$, $C_{33} \neq 0$, and $C_{66} = 1/2(C_{11} - C_{12}) \neq 0$.
[36] B. L. Hammond, W. A. Lester, and P. J. Reynolds Jr., *Monte Carlo Methods in Ab Initio Quantum Chemistry* (World Scientific, Singapore, 1994).
[37] R. Guardiola, Lect. Notes Phys. **510**, 269 (1998).
[38] D. M. Ceperley and M. H. Kalos, *Monte Carlo Methods in Statistics Physics* (Springer, Berlin, 1986).
[39] J. Boronat and J. Casulleras, Phys. Rev. B **49**, 8920 (1994).
[40] By related quantities is meant the expected value of operators $\hat{A}$ that commute with the Hamiltonian, namely, $[\hat{A}, \hat{H}] = 0$. It is also possible to obtain virtually exact results for $[\hat{A}, \hat{H}] \neq 0$ operators by using forward-walking-based techniques (see Refs. 41 and 42).
[41] R. Barnett, P. Reynolds, and W. A. Lester Jr., J. Comput. Phys. **96**, 258 (1991).
[42] J. Casulleras and J. Boronat, Phys. Rev. B **52**, 3654 (1995).
[43] R. A. Aziz, F. R. W. McCourt, and C. C. K. Wong, Mol. Phys. **61**, 1487 (1987).
[44] J. Boronat and J. Casulleras, Phys. Rev. B **49**, 8920 (1994).
[45] M. Zhai and Y.-S. Wu, J. Stat. Mech. (2005) P07003.
[46] C. Cazorla, G. Astrakharchick, J. Casulleras, and J. Boronat, New J. Phys. **11**, 013047 (2009).
[47] M. C. Gordillo, C. Cazorla, and J. Boronat, Phys. Rev. B **83**, 121406(R) (2011).
[48] S. A. Chin, Phys. Rev. A **42**, 6991 (1990).
[49] Y. Lutsyshyn, C. Cazorla, G. E. Astrakharchik, and J. Boronat, Phys. Rev. B **82**, 180506(R) (2010).
[50] Y. A. Freiman, S. M. Tretyak, A. Grechnev, A. F. Goncharov, J. S. Tse, D. Errandonea, H.-K. Mao, and R. J. Hemley, Phys. Rev. B **80**, 094112 (2009).
[51] S. Vitiello, K. Runge, and M. H. Kalos, Phys. Rev. Lett. **60**, 1970 (1988).
[52] S. Moroni, D. E. Galli, S. Fantoni, and L. Reatto, Phys. Rev. B **58**, 909 (1998).
[53] M. L. Klein, G. Chell, V. V. Goldman, and G. K. Horton, J. Phys. C: Solid State Phys. **3**, 806 (1970).
[54] J. B. Lurie, J. Low Temp. Phys. **10**, 751 (1973).
[55] M. J. P. Musgrave, Proc. R. Soc. London, Ser. A **226**, 339 (1954).
[56] V. V. Goldman, J. Low Temp. Phys. **36**, 521 (1979).
[57] H. J. Maris, J. Low Temp. Phys. **155**, 290 (2009).
[58] W. R. Gardner, J. K. Hoffer, and N. E. Phillips, Phys. Rev. A **7**, 1029 (1973).
[59] G. Ahlers, Phys. Rev. A **2**, 1505 (1970).
[60] In view of the experimental results reported in Fig. 10 of Ref. 3, this approximation can be considered as accurate enough.